ELSEVIER

International Journal of Refrigeration 23 (2000) 632–641

REVUE INTERNATIONALE DU FROID
INTERNATIONAL JOURNAL OF
refrigeration

www.elsevier.com/locate/ijrefrig

Modeling of integral-type Stirling refrigerator using system dynamics approach

B.J. Huang *, H.Y. Chen

Department of Mechanical Engineering, National Taiwan University, Taipei 106, Taiwan

Received 4 May 1998; received in revised form and accepted 6 December 1999

Abstract

A modeling of the integral-type Stirling refrigerator (ITSR) using a system dynamics approach is developed in the present study. The system dynamics models are derived to describe the input/output relation of each component of an ITSR. Connecting the equivalent circuits of the components together, we obtain a flow network diagram and derive a transfer function to represent system dynamics behavior of an ITSR. The performance analysis of an ITSR is then easily carried out by use of the transfer function with sinusoidal signal assumption. The performance calculation for a test refrigerator has shown that the analysis is accurate. An empirical correlation for a correction coefficient r in the expansion space was also derived for better results. The present study has demonstrated how a linear system theory or system dynamics approach can be applied to the design of an ITSR. © 2000 Elsevier Science Ltd and IIR. All rights reserved.

Keywords: Cryorefrigerator; Stirling; Design; Modelling

Modélisation d'un réfrigérateur Stirling de type intégré à l'aide d'une approche par dynamique du système

Résumé

Dans cette étude, on a effectué la modélisation d'un réfrigérateur Stirling de type intégré (ITSR) à l'aide d'une approche par dynamique du système. Les modèles de la dynamique du système sont développés afin de décrire la relation entrée/sortie de chaque composant d'un ITSR. En raccordant les circuits de composants, on obtient un diagramme pour l'écoulement en réseau avant de dériver une fonction de transfert qui représente le comportement dynamique du système d'un ITSR. L'analyse de la performance d'un ITSR devient alors facile grâce à l'utilisation de la fonction de transfert basée sur un signal sinusoïdal. Le calcul de la performance d'un réfrigérateur d'essai a ensuite montré que cette analyse est précise. Une corrélation empirique pour un coefficient de correction r *dans la chambre d'expansion a été dérivée afin d'obtenir de meilleurs résultats. Cette étude a montré qu'une théorie d'un système linéaire ou une approche par dynamique du système peut être appliquée à la conception d'un ITSR.* © 2000 Elsevier Science Ltd and IIR. All rights reserved.

Mots clés: Cryoréfrigérateur ; Stirling ; Conception ; Modélisation

* Corresponding author. Tel.: +886-2-2363-4790; fax: +886-2-2364-0549.
E-mail address: bjhuang@tpts6.seed.net.tw (B.J. Huang).

0140-7007/00/$20.00 © 2000 Elsevier Science Ltd and IIR. All rights reserved.
PII: S0140-7007(00)00003-7

Nomenclature

a_{dp}	gain of $G_{dp}(s)$
a_{ep}	gain of $G_{ep}(s)$
A	area (m^2)
C	flow capacitance (m^3 kg kJ^{-1})
C_p	specific heat at constant pressure (kJ kg^{-1} K^{-1})
C_v	specific heat at constant volume (kJ kg^{-1} K^{-1})
h	convection heat transfer coefficient (W m^{-2} K^{-1})
d	diameter (m)
f	frequency (Hz)
k	thermal conductivity (W m^{-1} K^{-1})
L	length (m)
m	mass flow rate (kg s^{-1})
R	gas constant (kJ kg^{-1} K^{-1})
Re	Reynolds number, dimensionless
p	pressure, Pa (N m^{-2})
P_{ch}	charge pressure, Pa (N m^{-2})
Q_{net}	net cooling capacity (W)
s	Laplace variable, complex
T	temperature (K)
t	time (s)
V	volume (m^3)
x	distance (m)
X	displacement (m)

Greek letters

ε	regenerator porosity, dimensionless
τ	time constant (s)
ω	angular frequency ($=2\pi f$) (rad s^{-1})
ρ	density (kg m^{-3})
θ	displacer leading angle to piston, deg

Subscripts

c	compression chamber; characteristic impedance; cold end
ce	cold end
d	displacer
e	expansion space
f	gas; fluid; flow
g	gas
h	hot end; hydraulic
H	hot end of the regenerator
i	inlet
L	cold end
m	mean; regenerator matrix
o	outlet; equilibrium point; amplitude
p	piston
r	regenerator
s	solid material
t	gas passage
w	warm space; cylinder wall

Superscripts

$\sim$	perturbed value

1. Introduction

An integral-type Stirling refrigerator (ITSR) comprises a compressor and a cold finger that are connected by a gas passage. The cold finger contains a moving regenerator/displacer, a cylinder, and an expansion space as shown in Fig. 1. Both the piston and the displacer motions are driven by a crank-shaft mechanism with a fixed phase angle between them. An electric motor drives the piston and hence the displacer such that the refrigerator operates approximately in a Stirling cycle. The physical processes involved in an ITSR includes thermodynamics, heat transfer of porous medium in the regenerator, gas transport in connecting tubes, tribology for the friction of piston and displacer motion. In addition, all the processes are at unsteady or cyclically-steady state. The thermal analysis of an ITSR is thus quite complicated.

Considerable work has been done by many researchers on the cycle analysis of the Stirling machine. The analysis basically utilizes the principle of thermodynamics and the conservation laws for mass, momentum and energy. The analysis is classified into two categories by Organ [1], engineering thermodynamics approach and flow-field approach. In either approach, a numerical calculation using the finite difference method is sometimes employed to calculate the cycle performance and the form of the solution is mostly for a single operating point in the performance envelope of a specific machine. A performance map for a specific machine is hardly obtained for the selection of an optimum operating condition.

Urieli and Berchowitz [2] treated a free-piston Stirling machine as a generalized single degree of freedom system (damped mass-spring system in mechanics) and derived the general relations for piston-displacer amplitude ratio and phase angle in terms of operating frequency. In order to carry out the cycle performance calculation, Urieli and Berchowitz [2] further used the closed-form solution of the isothermal analysis for the working gas pressure as a function of compression and expansion volume. The relations of piston-displacer amplitude ratio and phase angle for a specific machine were derived and used in the cycle performance calculation. Since the isothermal model is an ideal model, the analysis of Urieli and Berchowitz [2] for a free-piston Stirling machine will be inaccurate.

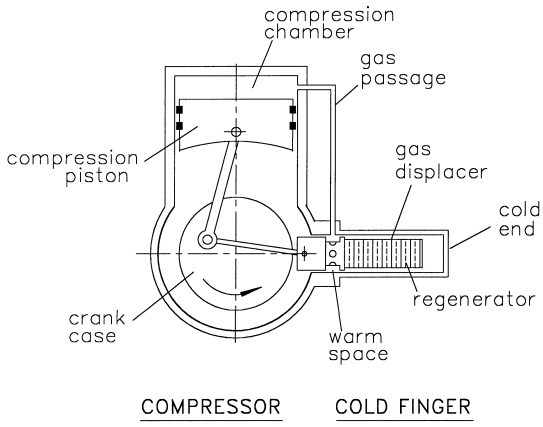

Fig. 1. Schematic diagram of an integral-type Stirling refrigerator.

Fig. 1. Schéma d'un réfrigérateur Stirling de type intégré.

For the analysis of an ITSR, a nodal model based on numerical computation scheme has been developed [3]. Several commercial software packages are available. However, the computation suffers easily from numerical problem and the accuracy in design is not known. In the present study, we intend to derive a model for the performance analysis of an ITSR that is different from the conventional approach in concept. A closed-form solution is obtained in transfer-function form and from which the performance of an ITSR is easily calculated.

Since an electric motor drives the piston and the displacer in sinusoidal motion approximately, a cyclically-steady state operation very close to sinusoidal is obtained in an ITSR. Every component of the refrigerator is thus subject to a sinusoidal signal and generates a sinusoidal output just like the frequency response of a dynamical system, from the point of view of system dynamics. A dynamics model can then be derived to describe the input/output relation of each component using the governing equations based on the conservation laws for mass, momentum and energy and the principle of thermodynamics. A linear system dynamics model can be further derived in conjunction with linearization and approximations. A system dynamics model and an equivalent system block diagram or equivalent circuit can then be used to represent the dynamics behavior of each component. Connecting the analogous circuits of all the components together will lead to a network representing the operation of the refrigerator.

Huang and Lu [4] derived two transfer functions for the split-type free-displacer Stirling refrigerator (STFSR). In the present study, we derived a transfer-function model of the ITSR for the system performance analysis.

The major difference between ITSR and STFSR is the driving mechanism of the displacer. The displacer of an ITSR is directly driven by a motor through a mechanism such as a crank-shaft mechanism. The displacer has a fixed stroke and a fixed phase angle with respect to the piston motion. For a STFSR, the displacer is driven by the fluid force or gaseous pressure which is indirectly induced by the piston motion. The stroke is thus variable and depends upon the operating conditions.

In modeling the ITSR by using a system dynamics approach, the piston displacement is the system input. The integral of the gas pressure in the expansion space with respect to the displacer motion is the gross refrigerating power that the refrigerator can obtain. The expansion-space pressure is, thus, the system output. That is, the refrigerator can be treated as a dynamical system with the piston displacement X_p as the system input and the gas pressure in the expansion space p_e as the system output. A transfer function representing the performance of the refrigerator can then be derived, from which the system performance can be easily evaluated at various operating points.

2. Dynamics model of components

Assuming that the working fluid is an ideal gas, we obtain the dynamics models of each component of an ITSR which are summarized as follows.

2.1. Compression chamber

Assuming an isothermal compression with a constant gas temperature T_c and no gas bypass between the piston and the cylinder, we obtain a dynamics model:

$$\dot{m}_p(s) \equiv \frac{sp_o A_p}{RT_c}\tilde{X}_p(s) = \dot{m}_c(s) + \frac{\tilde{p}_c(s)}{1/(sC_c)} \tag{1}$$

where $C_c = V_{co}/RT_c$ is the capacitance of the compression chamber. Here, $\dot{m}_p(s)$ acts as a current source representing the available or gross mass flowrate generated by the piston motion; $\dot{m}_c$ is the mass flowrate out of the compressor; p_c is the gas pressure inside the compression chamber; $V_c(t) = V_{co} - A_p X_p(t)$; V_{co} is the volume of the compression chamber for the piston at the equilibrium position; $X_p(t)$ is the piston displacement measured from the midpoint of the piston motion toward the top dead end; A_p is the cross-section area of the piston.

2.2. Gas passage

The gas passage links the compressor and the cold finger. Following the same treatment of Huang and Lu [4] for a connecting tube (assuming an isothermal process with a constant temperature T_t), we obtain a 1-D dynamics model of the passage:

$$\begin{bmatrix} \dot{m}_{\mathrm{to}}(s) \\ \tilde{p}_{\mathrm{to}}(s) \end{bmatrix} = \begin{bmatrix} \cosh(\Gamma_{\mathrm{t}} L_{\mathrm{t}}) & -\dfrac{1}{Z_{\mathrm{ct}}} \sinh(\Gamma_{\mathrm{t}} L_{\mathrm{t}}) \\ -Z_{\mathrm{ct}} \sinh(\Gamma_{\mathrm{t}} L_{\mathrm{t}}) & \cosh(\Gamma_{\mathrm{t}} L_{\mathrm{t}}) \end{bmatrix} \times \begin{bmatrix} \dot{m}_{\mathrm{ti}}(s) \\ \tilde{p}_{\mathrm{ti}}(s) \end{bmatrix} \tag{2}$$

where $\Gamma_{\mathrm{t}} = \sqrt{Z_{\mathrm{t}} Y_{\mathrm{t}}}$ and $Z_{\mathrm{ct}} = \sqrt{Z_{\mathrm{t}}/Y_{\mathrm{t}}}$ are the propagation constant and the characteristic impedance of the passage, respectively; $Z_{\mathrm{t}} = R_{\mathrm{Ft}} + sL_{\mathrm{Ft}} =$ series impedance and $Y_{\mathrm{t}} = sC_{\mathrm{Ft}} =$ shunt admittance;

$$\Gamma_{\mathrm{t}} = \sqrt{sC_{\mathrm{Ft}}(R_{\mathrm{Ft}} + sL_{\mathrm{Ft}})};\ Z_{\mathrm{ct}} = \frac{\Gamma_{\mathrm{t}}}{sC_{\mathrm{Ft}}} \tag{3}$$

where $C_{\mathrm{Ft}}, L_{\mathrm{Ft}}$ and R_{Ft} are the flow capacitance, flow inductance, and flow resistance per unit passage length, respectively, which are defined as

$$C_{\mathrm{Ft}} = \frac{A_{\mathrm{t}}}{RT_{\mathrm{t}}};\ L_{\mathrm{Ft}} = \frac{1}{A_{\mathrm{t}}};\ R_{\mathrm{Ft}} = \frac{\kappa}{A_{\mathrm{t}}} \tag{4}$$

where

$$\kappa = 0.1556(\rho_{\mathrm{t}} w_{\max} d_{\mathrm{t}}/\mu)^{-0.201}(w_{\max}/d_{\mathrm{h}}), \tag{5}$$

A_{t} is the cross-sectional area of the passage; $w_{\max}$ is the peak velocity of the oscillating flow in the passage; d_{t} is the hydraulic diameter of the passage. κ is considered to be a constant during the modeling, but should be adjusted by numerical iteration during the computation [4] to give a correct value for the corresponding mass flow $w_{\max}$.

2.3. Warm space

The gas in the warm space is assumed to be well-mixed at an uniform temperature. Similar to the compression chamber, a linearly perturbed model can be derived from mass continuity Eq. (4):

$$\dot{m}_{\mathrm{wi}}(s) = \frac{sp_{\mathrm{o}} A_{\mathrm{dw}}}{RT_{\mathrm{w}}} X_{\mathrm{d}}(s) + \dot{m}_{\mathrm{wo}}(s) + \frac{\tilde{p}_{\mathrm{w}}(s)}{1/(sC_{\mathrm{w}})} \tag{6}$$

where $C_{\mathrm{w}} = V_{\mathrm{wo}}/(RT_{\mathrm{w}})$. The first term in the right-hand side of Eq. (6) is the mass flowrate induced by the displacer motion, which is analogous to an electric current source; the third term represents the flow capacitance effect of the warm space.

2.4. Regenerator

The regenerator is an energy-storage element made from packed wire screens. Assuming 1-D flow, no axial conduction and constant properties, Huang and Lu [4,5] obtained the dynamics model of the regenerator:

$$\begin{bmatrix} \dot{m}_{\mathrm{ro}}(s) \\ \tilde{p}_{\mathrm{ro}}(s) \end{bmatrix} = R(s) \times \begin{bmatrix} \dot{m}_{\mathrm{ri}}(s) \\ \tilde{p}_{\mathrm{ri}}(s) \end{bmatrix} \tag{7}$$

where

$$R(s) = \begin{bmatrix} R_{\mathrm{mm}}(s) & R_{\mathrm{mp}}(s) \\ R_{\mathrm{pm}}(s) & R_{\mathrm{pp}}(s) \end{bmatrix} \tag{8}$$

$$\begin{aligned} R_{\mathrm{mm}}(s) &= R_{\mathrm{pp}}(s) = \cosh[\Gamma_{\mathrm{r}}(s) L_{\mathrm{r}}] \\ R_{\mathrm{mp}}(s) &= -\frac{\sinh[\Gamma_{\mathrm{r}}(s) L_{\mathrm{r}}]}{Z_{\mathrm{cr}}(s)} \\ R_{\mathrm{pm}}(s) &= -Z_{\mathrm{cr}}(s) \sinh[\Gamma_{\mathrm{r}}(s) L_{\mathrm{r}}] \end{aligned} \tag{9}$$

where $\Gamma_{\mathrm{r}} = \sqrt{Z_{\mathrm{r}} Y_{\mathrm{r}}}$ and $Z_{\mathrm{cr}} = \sqrt{Z_{\mathrm{r}}/Y_{\mathrm{r}}}$ are the propagation constant and the characteristic impedance of the regenerator, respectively; $Z_{\mathrm{r}} = R_{\mathrm{Fr}} + sL_{\mathrm{Fr}} =$ series impedance and $Y_{\mathrm{r}} = sC_{\mathrm{Fr}} =$ shunt admittance;

$$\Gamma_{\mathrm{r}} = \sqrt{sC_{\mathrm{FTr}}(R_{\mathrm{Fr}} + sL_{\mathrm{Fr}})};\ Z_{\mathrm{cr}} = \frac{\Gamma_{\mathrm{r}}}{sC_{\mathrm{FTr}}} \tag{10}$$

where C_{FTr} is the regenerator flow capacitance due to pressure change and time responses of gas and matrix:

$$C_{\mathrm{FTr}} = C_{\mathrm{Fr}} \frac{1 + \tau_{\mathrm{sr}}/[\tau_{\mathrm{gr}}(1 + s\tau_{\mathrm{sr}})]}{\gamma + \tau_{\mathrm{sr}}/[\tau_{\mathrm{gr}}(1 + s\tau_{\mathrm{sr}})]} \tag{11}$$

where $\gamma = C_{\mathrm{p}}/C_{\mathrm{v}}$; C_{Fr} and C_{Tr} are the flow capacitance per unit length due to pressure and temperature changes, respectively; L_{Fr} and R_{Fr} are flow inductance, and flow resistance per unit length, respectively. They are defined as

$$C_{\mathrm{Fr}} = \frac{A_{\mathrm{fr}}}{RT_{\mathrm{rm}}};\ C_{\mathrm{Tr}} = \frac{p_{\mathrm{rm}} A_{\mathrm{fr}}}{RT_{\mathrm{rm}}^2};\ L_{\mathrm{Ft}} = \frac{1}{A_{\mathrm{fr}}};\ R_{\mathrm{Fr}} = \frac{\bar{\alpha}\varepsilon\nu}{A_{\mathrm{fr}}} \tag{12}$$

where

$$\bar{\alpha} = \alpha + (\beta/d_{\mathrm{h}})\varepsilon \mathrm{Re}_{\mathrm{h}};\ \alpha = 175/(2\varepsilon d_{\mathrm{h}}^2);\ \beta = 1.6/(2\varepsilon^2 d_{\mathrm{h}});$$

$$d_{\mathrm{h}} = \varepsilon d_{\mathrm{m}}/(1-\varepsilon);\ h = 0.33(k_{\mathrm{f}}/d_{\mathrm{h}})\mathrm{Re}_{\mathrm{h}}^{0.67}$$

$$\tau_{\mathrm{gr}} = \frac{p_{\mathrm{rm}} \varepsilon V_{\mathrm{o}} C_{\mathrm{v}}}{RT_{\mathrm{rm}} h A_{\mathrm{HT}}};\ \tau_{\mathrm{sr}} = \frac{\rho_{\mathrm{s}}(1-\varepsilon) V_{\mathrm{o}} C_{\mathrm{s}}}{h A_{\mathrm{HT}}}$$

A_{HT} is the surface area of the regenerator $= 4V_{\mathrm{o}}(1-\varepsilon)/d_{\mathrm{m}}$; Re_{h} is the Reynolds number based on hydraulic diameter d_{h}; k_{f} is the thermal conductivity of the gas.

Eq. (7) represents the dynamics model of the regenerator in terms of the pressure and mass flowrate that are derived from the continuity and momentum equations. The gas temperature at the cold side of the regenerator is derived as [4]

$$\tilde{T}_{\mathrm{fr}}(L_{\mathrm{r}}, s) = -\frac{C_{\mathrm{Fr}}}{C_{\mathrm{Tr}}}\frac{\tau_{\mathrm{gr}}(1+s\tau_{\mathrm{sr}})}{\tau_{\mathrm{sr}}}\tilde{p}_{\mathrm{ro}}(s) - \frac{\gamma}{C_{\mathrm{Tr}}}\frac{\tau_{\mathrm{gr}}(1+s\tau_{\mathrm{sr}})\Gamma_{\mathrm{r}}(s)}{s\tau_{\mathrm{sr}}\sinh[\Gamma_{\mathrm{r}}L_{\mathrm{r}}]} \times [\dot{m}_{\mathrm{ro}}(s)\cosh(\Gamma_{\mathrm{r}}L_{\mathrm{r}}) - \dot{m}_{\mathrm{ri}}(s)]. \tag{13}$$

2.5. Displacer

The displacer of an ITSR is driven by a crank-shaft mechanism (Fig. 1). The time functions for the displacer and piston motion are approximately sinusoidal. Therefore,

$$X_{\mathrm{d}}(t) = X_{\mathrm{do}}\sin(\omega t + \theta)$$
$$X_{\mathrm{p}}(t) = X_{\mathrm{po}}\sin(\omega t)$$

where X_{do} and X_{po} are the amplitudes of the displacer and the piston, respectively; θ is the phase lead of the displacer. Thus, a transfer function $G_{\mathrm{dp}}(s)$ for the displacer motion can be derived as

$$G_{\mathrm{dp}}(s) = \frac{X_{\mathrm{d}}(s)}{X_{\mathrm{p}}(s)} = \frac{X_{\mathrm{do}}}{X_{\mathrm{po}}}\mathrm{e}^{s\theta} \tag{14}$$

2.6. Expansion space

The expansion space is usually an empty space for the gas to expand and absorb heat from the environment. Huang and Lu [4] derived a dynamics model from the mass continuity equation. To take into account the gas bypass from the displacer clearance, we modify the flow capacitance $C_{\mathrm{e}}(= V_{\mathrm{eo}}/RT_{\mathrm{ee}})$ with a correction coefficient r and obtain the dynamics equation:

$$\dot{m}_{\mathrm{e}}(s) = \frac{\tilde{p}_{\mathrm{e}}(s)}{1/(rsC_{\mathrm{e}})} - \frac{sp_{\mathrm{o}}A_{\mathrm{de}}}{RT_{\mathrm{ce}}}\tilde{X}_{\mathrm{d}}(s) \tag{15}$$

The second term in the right-hand side of Eq. (15) is the mass flowrate induced by the displacer motion, which is analogous to a current source. The correction coefficient r represents the gas bypass from the displacer clearance. The amount of gas bypass is related to the seal design, manufacturing process, material used and operating condition. The relation of r can be determined empirically. $r = 1$ represents no gas bypass in the expansion space.

3. Analogous network of integral-type stirling refrigerator

Combining the equivalent circuits or block diagrams of all the components according to the process of ITSR, we obtain the analogous network as shown in Fig. 2.

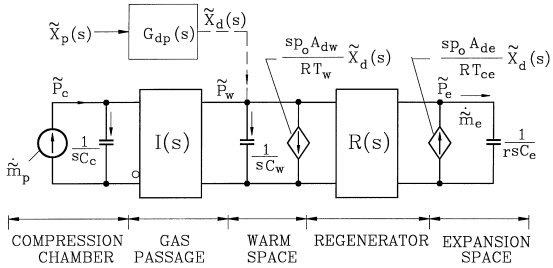

Fig. 2. Linear network of integral-type Stirling refrigerator.

Fig. 2. Réseau linéaire du réfrigérateur Stirling de type intégré.

The lower part of Fig. 2 is the fluid network in which mass flow is analogous to current and pressure is analogous to voltage. The fluid network depicts the gaseous flow propagation from the compressor to the expansion space. The upper part of Fig. 2 represents the displacer model which responds the piston motion by a phase angle θ and transfers the displacer displacement signal $\tilde{X}_{\mathrm{d}}$ to the fluid network. Since the displacer motion is fixed and follows the piston motion by a phase angle, we can solve the fluid network to find the gas flowrate and pressure at each component.

4. Transfer function of integral-type stirling refrigerator

We draw only block diagram in Fig. 2 for the gas passage and the regenerator since their dynamics models belong to distributed-parameter type. The transfer function of the ITSR is derived by combining the above equations:

$$G_{\mathrm{ep}}(s) = \frac{\tilde{p}_{\mathrm{e}}(s)}{X_{\mathrm{p}}(s)} = G_9(s) + G_{10}(s)G_{\mathrm{dp}}(s) \tag{16}$$

where

$$G_{\mathrm{dp}}(s) = \frac{X_{\mathrm{d}}(s)}{X_{\mathrm{p}}(s)} = \frac{X_{\mathrm{do}}}{X_{\mathrm{po}}}\mathrm{e}^{s\theta} \tag{14}$$

$$G_{10}(s) = \frac{G_6(s) - G_7(s)E_{\mathrm{md}}(s)}{G_8(s) + G_7(s)E_{\mathrm{me}}(s)} \tag{17}$$

$$G_9(s) = \frac{1}{G_8(s) + G_7(s)E_{\mathrm{me}}(s)} \tag{18}$$

$$G_8(s) = -G_3(s)R_{\mathrm{mp}}(s) + G_5(s)R_{\mathrm{mm}}(s) \tag{19}$$

$$G_7(s) = G_3(s)R_{\mathrm{pp}}(s) - G_5(s)R_{\mathrm{pm}}(s) \tag{20}$$

$$G_6(s) = G_3(s)W_{\mathrm{md}}(s) \tag{21}$$

$$G_5(s) = G_4(s) - G_3(s)W_{\mathrm{mp}}(s) \tag{22}$$

$$G_4(s) = -G_1(s)I_{\mathrm{mp}}(s) + G_2(s)I_{\mathrm{mm}}(s) \tag{23}$$

$$G_3(s) = G_1(s)I_{pp}(s) - G_2(s)I_{pm}(s) \tag{24}$$

$$G_2(s) = \frac{C_{mc}(s)}{C_{mp}(s)}; \quad G_1(s) = \frac{1}{C_{mp}(s)} \tag{25}$$

$$C_{mp}(s) = \frac{sp_oA_p}{RT_c}; \quad C_{mc}(s) = sC_c \tag{26}$$

$$W_{mp}(s) = -\frac{sV_{wo}}{RT_w}; W_{md}(s) = -\frac{sp_oA_{dw}}{RT_w} \tag{27}$$

$$E_{me}(s) = \frac{rsV_{eo}}{RT_{ce}}; E_{md}(s) = -\frac{sp_oA_{de}}{RT_{ce}} \tag{28}$$

$$I_{mm}(s) = I_{pp}(s) = \cosh[\Gamma_t(s)L_t]; \tag{29}$$

$$I_{mp}(s) = -\frac{\sinh[\Gamma_t(s)L_t]}{Z_{ct}(s)}; I_{pm}(s) = -Z_{ct}\sinh[\Gamma_t(s)L_t] \tag{30}$$

It is seen that the system input of an ITSR is the piston displacement X_p of the compressor. The system output is the expansion space pressure p_e. The integral-type Stirling refrigerator thus belongs to a single-input-single-output (SISO) dynamical system.

5. Performance calculation

5.1. Maximum available cooling capacity

The maximum available cooling capacity of an ITSR can be evaluated by integrating the expansion space pressure $p_e(t)[=\bar{p}_e + \tilde{p}_e(t)]$ with respect to volume $V_e(t)$, where $V_e(t)$ is related to the displacer displacement $X_d(t)$. For a given piston and displacer motion, $X_p(t)$ and $X_d(t)$, according to the crank-shaft mechanism design, $\tilde{p}_e(t)$ can be obtained from the inverse of the transfer function $G_{ep}(s)$, Eq. (16). The computation procedure is however quite complicated. A simplification is needed. Since the piston is driven by a crank-shaft mechanism, the piston and the displacer motion as well as the induced pressure and mass flow waves inside the refrigerator approaches sinusoidal with the time functions of $X_d(t)$ and $\tilde{p}_e(t)$ expressed as

$$\tilde{p}_e(t) = p_{eo}\sin(\theta + \phi_e) \tag{31}$$

$$X_d(t) = X_{do}\sin(\theta + \phi_d)$$

where p_{eo} and X_{do} are the amplitudes of the expansion space pressure and the displacer, respectively; ϕ_e and ϕ_d are the phase lead angles of $p_e(t)$ and $X_d(t)$ with respect to the piston motion. The amplitude of the expansion space pressure can then be expressed as

$$\begin{aligned} p_{eo} &= |G_{ep}(j\omega)||X_p(j\omega)| = a_{ep}X_{po} \\ X_{do} &= |G_{dp}(j\omega)||X_p(j\omega)| = a_{dp}X_{po} \end{aligned} \tag{32}$$

The maximum cooling capacity Q_{max} thus can be computed simply from the gains of the frequency response functions $G_{ep}(j\omega)$ and $G_{dp}(j\omega)$, i.e. a_{ep} and a_{dp}, and the phase angles of $X_d(t)$ and $p_e(t)$, i.e. ϕ_e and ϕ_d:

$$\begin{aligned} Q_{max} &= f\int_0^{2\pi} p_e dV_e = f\pi p_{eo}A_{de}X_{do}\sin(\phi_d - \phi_e) \\ &= f\pi a_{ep}a_{dp}X_{po}^2A_{de}\sin(\phi_d - \phi_e) \end{aligned} \tag{33}$$

where A_{de} is the cross-section area of the displacer.

5.2. Net cooling capacity

The net cooling capacity of an ITSR can be evaluated by subtracting the heat losses from the maximum available cooling capacity. There are three types of heat losses: namely, regenerator heat conduction loss Q_{cond}, regenerator enthalpy flow loss Q_{enth}, and displacer shuttle heat loss Q_{shutt}. Thus the net cooling capacity is

$$Q_L = Q_{max} - Q_{shutt} - Q_{cond} - Q_{enth} \tag{34}$$

where

$$Q_{cond} = k_{eff}(\pi D_r^2/4)\frac{T_H - T_L}{L_r} \tag{35}$$

$$\begin{aligned} Q_{enth} &= f\oint m_{ro}(t)C_pT_{fr}(L_r, t)dt \\ &= f\pi C_p|\tilde{m}_{ro}||\tilde{T}_{fr}(L_r)|\cos(\phi_m - \phi_T) \end{aligned} \tag{36}$$

where k_{eff} is the effective thermal conductivity of the regenerator; D_r is the regenerator diameter; L_r is the regenerator length; T_H and T_L are the temperature at the hot and cold ends of the regenerator; ϕ_m and ϕ_T are, respectively, the phases of $m_{ro}(t)$ and $\tilde{T}_{fr}(L_r, t)$. $\tilde{T}_{fr}(L_r, t)$ follows Eq. (13). The displacer/regenerator shuttle heat loss is evaluated from the relation of Baik and Chang [6]:

$$Q_{shutt} = \frac{\pi D_eS_e}{4}2\pi f \quad k_d\rho_dC_{pd}T_{10}\sin\phi \tag{37}$$

where

$$T_{10} = \Delta T_dS_e\frac{a_2}{\sqrt{\left(\frac{a_1+a_2}{\sqrt{2}}\right)^2 + \left(\frac{a_1+a_2}{\sqrt{2}} + a_1a_2\right)^2}} \tag{38}$$

$$\phi = \tan^{-1}\left(\frac{\frac{a_1+a_2}{\sqrt{2}} + a_1a_2}{\frac{a_1+a_2}{\sqrt{2}}}\right) \tag{39}$$

$$a_1 = \frac{k_d}{h}\sqrt{\frac{2\pi f}{\alpha_d}}; \quad a_2 = \frac{k_w}{h}\sqrt{\frac{2\pi f}{\alpha_w}} \tag{40}$$

where D_e is the displacer outside diameter; S_e is the displacer stroke; k_d is the displacer thermal conductivity; k_w is the cylinder wall thermal conductivity; ρ_d is the displacer density; C_{pd} is the displacer heat capacity; ΔT_d is the axial temperature gradient of the displacer; α_d and $\alpha_w$are the thermal diffusivity of the displacer and the cylinder wall; h is the heat transfer coefficient.

The gas bypass loss at the clearance between the displacer and the cylinder wall is related to the seal design, manufacturing process, material used, and operating condition. A correction coefficient r is introduced in the expansion space model, Eq. (15), to account for this effect.

5.3. Refrigerator COP

The COP of the integral-type Stirling refrigerator can be evaluated by the relation:

$$COP = \frac{Q_L}{W_{comp}} \tag{41}$$

where

$$W_{comp} = f\oint p_c dV_c \tag{42}$$

For simplification, the compression work computed from the above equation does not take into account the motor efficiency.

6. System design analysis and experimental verification

The system design analysis of an ITSR can be carried out using the present model. For simplification, the following assumptions are made in the analysis:

1. Since the mixing is severe in the compression space, the gas temperature in the compressor can be assumed uniform. The gas temperature inside the gas passage is also assumed uniform since it is very short in ITSR. Therefore, the regenerator inlet temperature T_{ri} approximates the gas temperature in the compression chamber T_c and in the passage T_t, i.e. $T_{ri} \approx T_t \approx T_c$.
2. The gas temperature of the warm space is constant and equal to the outside wall surface temperature T_H and the regenerator inlet temperature T_{ri}. That is, $T_w \approx T_{ri} \approx T_H$.
3. The gas temperature in the cold space (expansion space) T_{ce} is approximately equal to the outside wall temperature of the cold end, T_L. That is, $T_{ce} \approx T_L$.
4. The mean pressure p_o is equal to the charge pressure P_{ch}.
5. The wall temperatures at the two ends of the regenerator, T_{ri} and T_{ro}, are approximately constant. Thus, $T_w \approx T_{ri} \approx T_t \approx T_c$; $T_{ro} \approx T_{ce} \approx T_L$.

Table 1
Design specifications of a test refrigerator

Tableau 1
Spécifications pour la conception d'un réfrigérateur d'essai

1.	*Compressor*	
	Piston diameter	14 mm
	Piston stroke	2 mm
	Connecting rod length	17 mm
2.	*Gas passage*	
	Length	25 mm
	Inside diameter	1.5 mm
3.	*Warm space*	
	Volume	0.5 c.c.
4.	*Regenerator*	
	Wire screen material	SS316
	Wire screen mesh no.	500
	Wire screen length	37 mm
	Wire screen diameter	4 mm
	Number of screen disks	740
5.	*Displacer*	
	Stroke	2.0 mm
	Connecting rod length	20.6 mm
	Diameter	6.15 mm
6.	*Expansion space*	
	Diameter	6.15 mm
	Dead space length	1.5 mm
7.	*Design-point operating conditions*	
	Charge pressure	13.6 kg/cm^2 gage
	Frequency	35 Hz
	Cold-end temperature	80 K
	Net cooling capacity	0.2 W

Table 2
Measured and calculated cooling capacity at $P_{ch} = 13.6$ kg/cm^2 gage; f = 35 Hz

Tableau 2
Puissance frigorifique mesurée et calculée sous des conditions P_{ch} *= 13,6 kg/cm^2 ; f = 35 Hz*

Cold-end temp T_L, K	Net cooling capacity Q_L, W	
	Calculated	Measured
58	0.126	0
69	0.152	0.100
76	0.167	0.150
82	0.180	0.200
90	0.196	0.250

Given the refrigerator dimensions, the material physical properties, the operating conditions (T_L, P_{ch}, f, T_c, T_w), and the working fluid properties, we can carry out the system performance analysis using the present model. It takes several seconds for each run on PC586.

We carry out a performance calculation for a test refrigerator with design specifications listed in Table 1. High purity helium gas is used as the working fluid. The test refrigerator is designed to operate with 0.2 W cooling capacity at 35 Hz and 14.6 kg/cm^2 abs charge pressure.

Table 2 shows that the measured net cooling capacity is very close to the calculated value from the assumption of $r = 1$ in Eq. (15) , i.e. no gas bypass in the expansion space. It can be seen from Fig. 3 that the predicted value coincides with the measured value at the design point. The deviation between the measured and the calculated values however is larger at the off-design conditions. This may result from the gas bypass in the expansion space due to the variation of displacer clearance caused by the temperature change. The displacer casing of the test ITSR is made from a plastic material that may have a shrinkage different from the cylinder wall material (stainless steel) over different T_L.

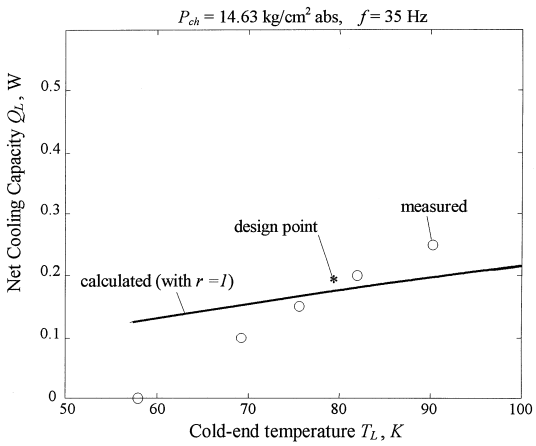

Fig. 3. Measured and calculated cooling capacity vs cold-end temperature.

Fig. 3. Puissance frigorifique mesurée et calculée en fonction de la température de l'extrémité froide.

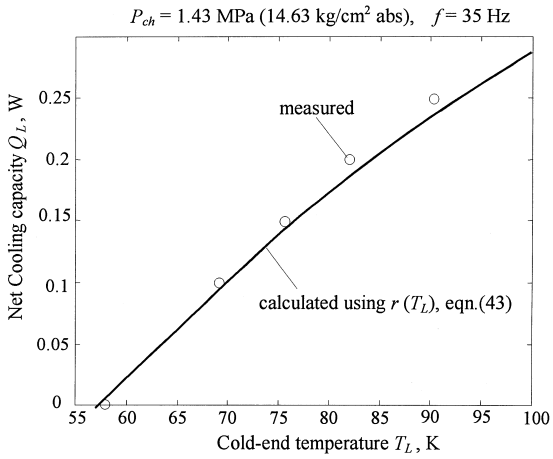

Fig. 5. Comparison of measured cooling capacity with calculated results.

Fig. 5. Comparaison de la puissance frigorifique mesurée et des résultats calculés.

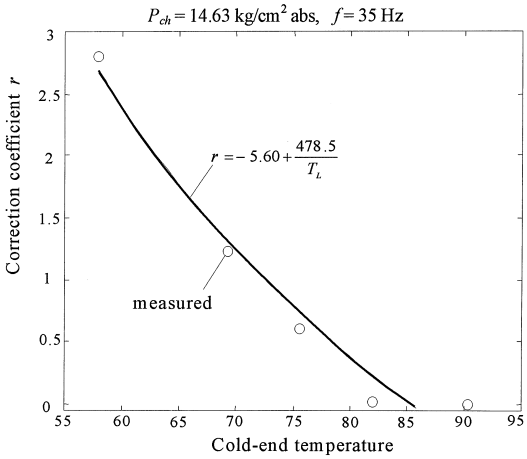

Fig. 4. Gas bypass correction coefficient.

Fig. 4. Coefficient de correction de la dérivation du gaz.

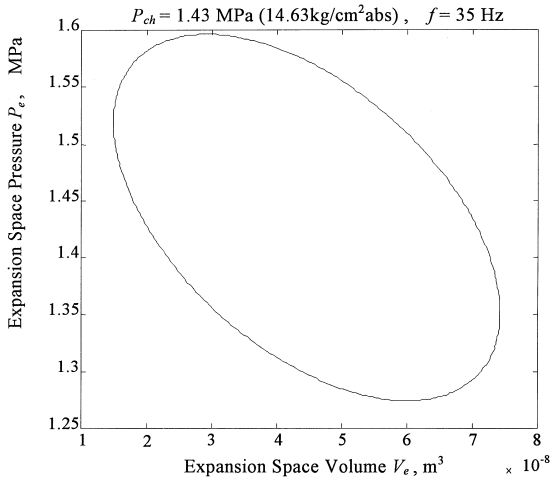

Fig. 6. Calculated expansion space PV diagram.

Fig. 6. Diagramme pression-volume de la chambre d'expansion.

The correction coefficient r is determined by adjusting its value so as to fit the calculated Q_L to the measured Q_L. Fig. 4 shows the determined value of r. An empirical correlation is derived for $P_{ch} = 1.43\text{MPa}\,(14.63\text{kg/cm}^2)$ and $f = 35$ Hz:

$$r = -5.60 + \frac{478.5}{T_L} \tag{43}$$

The predicted net cooling capacity coincides with the test results, as shown in Fig. 5, if the correction coefficient relation, Eq. (43), was used. Figs. 6 and 7 are, respectively, the PV diagram and the COP of the refrigerator predicted from the present analysis. The correction coefficient r may vary with the operating frequency, in addition to the cold-end temperature. A more general empirical correlation of r is also derived from the analysis of test data:

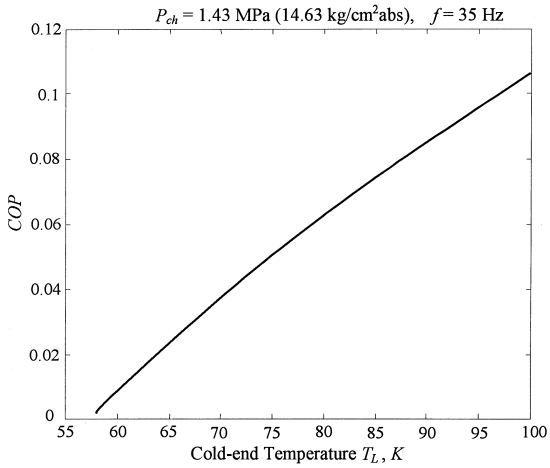

Fig. 7. Calculated COP vs cold-end temperature.

Fig. 7. COP calculé en fonction de la température de l'extrémité froide.

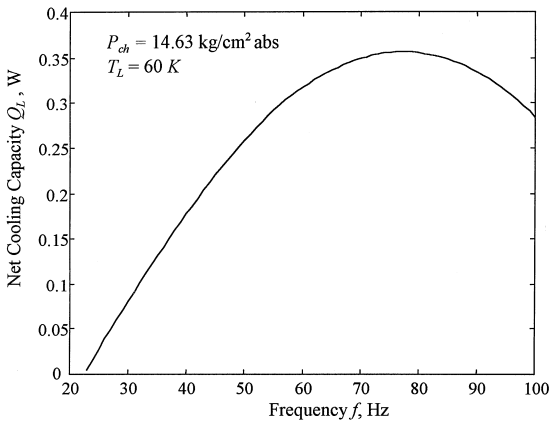

Fig. 8. Prediction of net cooling capacity variation with operating frequency.

Fig. 8. Prévision des variations de puissance frigorifique nette selon la fréquence de fonctionnement utilisée.

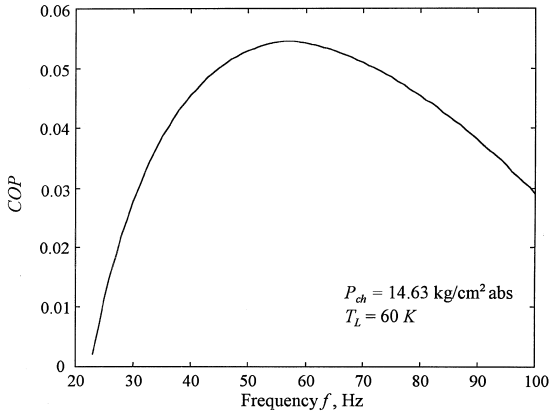

Fig. 9. Prediction of COP variation with operating frequency.

Fig. 9. Prévision de la variation du COP selon la fréquence de fonctionnement utilisée.

Table 3
Comparison of measured and calculated cold-end temperature at various operating conditions (all with $P_{ch} = 1.43$MPa)

Tableau 3
Comparaison des températures d'extrémité froide mesurées et calculées sous diverses conditions de fonctionnement (dans tous les cas avec P_{ch} = 1,43 MPa)

Net cooling capacity Q_L, W	Frequency, Hz	Cold-end temperature, K		Calculated-measured, K
		Calculated	Measured	
0	35	57.3	57.9	−0.6
	40	54.0	56.5	−2.5
	45	54.0	56.5	−2.5
	50	50.7	55.0	−4.3
0.10	35	69.8	69.2	0.6
	40	64.9	64.0	0.9
	45	61.7	61.4	0.3
	50	59.6	59.7	−0.1
0.15	35	76.6	75.6	1.0
	40	70.6	68.6	2.0
	45	66.6	65.8	0.8
	50	64.1	63.8	0.3
0.20	35	84.2	82.0	2.2
	40	76.8	74.3	2.5
	45	71.9	70.4	1.5
	50	73.4	72.1	1.3
0.25	35	92.8	90.3	2.5
	40	83.5	79.8	3.7
	45	77.4	75.2	2.2
	50	73.4	72.1	1.3

$$r = \left[-5.988 + \frac{478.5}{T_L}\right] \times \left(1.589 - 3.6211 \times 10^{-2} f + 5.5041 \times 10^{-4} f^2\right) \quad (44)$$

where T_L is in K; f is in Hz.

Table 3 shows the comparison between measured and calculated T_L of the test refrigerator. It is shown that all the deviations are within $\pm 5K$, mostly within $\pm 3K$.

7. Discussion and conclusion

The performance calculation of an ITSR may not be so difficult. If we look at the performance of an ITSR from the point of view of system dynamics, the modeling can be greatly simplified. It is shown in the present study that a transfer function can be derived to represent the system dynamics behavior of an ITSR and from which the thermal performance can be evaluated with sinusoidal signal assumption. The computation on PC586 just takes a few seconds for a design calculation. The performance calculation for a test refrigerator has shown that the analysis is accurate at the design point. An empirical correlation for the correction coefficient r in the expansion space was also derived in the present study for better results at off-design conditions. A PC-based computer package was also developed in the present study so that engineer can easily use it for design purposes. The modeling can be improved furthermore by applying a better oscillating-flow heat transfer and frictional correlation for the regenerator and the gas passage, if they are available. It is also noticeable that the manufacturing quality and the material selected for the displacer, the regenerator, and the cylinder wall are crucial. Any moderate defect during manufacturing will cause the performance to deviate largely from the prediction. The correction coefficient r reflects to some extent on this factor and the function would depend largely on individual overall engineering capability. Finally, it should be emphasized that the present study has demonstrated how a linear system theory or system dynamics approach can be applied to the design of an ITSR. This approach enables us to draw a performance map of a specific ITSR at various operating conditions and study the optimum design. The performance calculation follows the frequency-response analysis and presents the performance over all operating frequencies. Figs. 8 and 9 are the prediction of Q_L and COP for the present test ITSR operated at $P_{ch} = 14.63$ kg/cm^2 abs and $T_L = 60$K. It is seen that an optimum operating frequency can be determined with respect to either the maximum net cooling capacity Q_L or the maximum COP. If we repeated the same calculation of Figs. 8 and 9 for different P_{ch} or T_L, we can draw a performance map for a specific ITSR for design selection.

Acknowledgements

The present study was supported by the National Science Council, Taiwan, through the Grant No.NSC81-0401-E002-587, No.CS83-0210-D-002-011 and No.CS84-0210-D-002-027.

References

[1] Organ AJ. Thermodynamics and gas dynamics of the stirling cycle machine. Cambridge: Cambridge University Press, 1992 (chapter 4).
[2] Urieli I, Berchowitz DH. Stirling cycle engine analysis. Bristol, UK: Adam Hilger Ltd, 1984.
[3] Yuan SWK, Spradley IE, Yang PM, Nast TC. Computer simulation model for Lucas Stirling refrigerators. Cryogenics 1992;32:143–8.
[4] Huang BJ, Lu CW. Split-type free-displacer Stirling refrigerator design using linear network analysis. Cryogenics 1996;36:1005–17.
[5] Huang BJ, Lu CW. Linear network analysis of regenerator in a cyclic-fkiw system. Cryogenics 1995;35:203–7.
[6] Baik JH, Chang HM. An exact solution for shuttle heat transfer. Cryogenics 1995;35:9–13.